International Journal of Precision Engineering and Manufacturing (2020) 21:983–993
https://doi.org/10.1007/s12541-020-00329-5

Online ISSN 2005-4602
Print ISSN 2234-7593

REGULAR PAPER

A Novel Approach to Separate Geometric Error of the Rotary Axis of Multi-axis Machine Tool Using Laser Tracker

Jindong Wang[1] · **Cong Cheng**[1] · **Haitao Li**[2]

Received: 8 November 2019 / Revised: 29 January 2020 / Accepted: 29 January 2020 / Published online: 7 February 2020

Abstract

It is highly desirable to enhance machining accuracy for multi-axis machine tool, in which the geometric accuracy of rotary axis is a main contributing factor. Thus, how to achieve the fast and accurate identification of each geometric error of rotary axis, as well as its correction and compensation has become a key issue. This paper presents a novel method of geometric error separation of the rotary axis by means of laser tracker. For this method, the direction variation of the vectors composed by some adjacent measuring points during the rotation of turntable is measured, and rotary axis's six geometric errors including three linear displacement and three angular displacement errors can be accurately identified on the basis of the mapping relationship between the vector's direction variation and each geometric error. Meanwhile, the multi-station and time-sharing measurement is adopted based on GPS principle, aiming to overcome the effect of angle measurement error using laser tracker. Eventually, the geometric error separation mathematical model on rotary axis with this novel method is established, and the corresponding measurement algorithms containing the base station calibration and the measuring point determination based on the hybrid genetic algorithm, as well as each geometric error separation algorithm are deduced respectively. Furthermore, the numerical simulations are conducted to examine the validity of the derived algorithms. Results of the comparative experiment demonstrate that high-efficiency and high-precision measurement for the geometric error of the rotary axis can be accomplished by the proposed approach.

Keywords Laser tracker · Rotary axis · Error identification · Measurement algorithm

Lists of Symbols

$\delta_x(\theta)$	Linear displacement error of C-axis in X direction
$\varepsilon_x(\theta)$	Angular displacement error of C-axis around X-axis
T_1	Theoretical transformation matrix
T_2	Error transformation matrix
A_0	Initial measuring point
$\overrightarrow{A_iB_i}$	Vector formed by measuring points A_i and B_i
P_1	Position of the first base station
l_{1i}	Distance from the base station P_1 to measuring point A_i
Δl_{1i}	Change of distance from the base station P_1 to measuring point A_i

✉ Jindong Wang
wangjindong@swjtu.edu.cn

Cong Cheng
chengccxc@foxmail.com

Haitao Li
pirate328@163.com

[1] School of Mechanical Engineering, Southwest Jiaotong University, Chengdu 610031, China

[2] College of Mechanical and Electrical Engineering, Shaanxi University of Science and Technology, Xi'an 710021, China

1 Introduction

With the increased machining accuracy and workpiece complexity, the importance of multi-axis CNC machine tools is becoming growingly prominent in the manufacturing industry. It enables efficient machining of complex parts by adding rotating parts on conventional three-axis type [1–3]. The machining accuracy is the main performance index for NC machine tools, and how to further elevate it has become a research hotspot. For the multi-axis machining, the geometric error of its rotary axis has a great influence on the overall machining accuracy, which can be improved effectively through measuring and compensating the corresponding errors. However, how to quickly and accurately identify it becomes a key scientific problem that has direct impact on the compensation effect [4–9].

At present, there are various ways to separate the linear axis' geometric errors of multi-axis machine tool, and the measurement technology is relatively mature. Whereas, study on detecting the rotary axis errors is rarely involved as a research difficulty [10], especially for simultaneous separation of the six geometric errors. The autocollimator, laser ball bar and R-test are generally used to detect the rotary axis errors. Combining an autocollimator with a polygon, the rotary axis's position error can be assessed, but it's not available for other errors evaluation. When measured with the ball bar, the remaining five geometric errors except the position error can be identified via the axial double-loop test and the cone test. Zargarbashi and Mayer, designed the five measurement modes based on the ball bar's sensitive direction to detect A-axis's motion error [11]. However, the interaction of multi-axis linkage and multi-mode measurement are required, making the measurement process and error identification model more complicate by this method. In addition, R-test was also adopted to measure the position-dependent geometric errors of rotary axis [12]. Then the multi-axis linkage and high-precision measuring devices are all required, which limits its application to a certain extent.

Since the 1980 s, the laser tracking measurement technology has rapid growth to meet the increasing needs of motion measurement of industrial robots, detection and assembly for some large workpieces, and so on [13–16]. With fast, dynamic and portable performance, the laser tracker now has been widely applied to large-scale metrology fields such as aerospace, ships, and automobiles. Currently, it is also applied to machine tool precision detecting [17–20].

In this work, the laser tracker is applied to realize rapid and accurate detection of the rotary axis's geometric errors for the multi-axis NC machine tool. To overcome the influence of angle measurement error introduced by using the laser tracker, the multi-station and time-sharing measurement is adopted based on GPS principle. Then a novel separation method for the rotary axis's six geometric errors is proposed in this investigation. Taking the identification of the turntable's geometric errors as a precedent, the direction variations of the composed vectors during the rotation of turntable is measured, and the mutual mapping relationship is then established between the variations in the vector's direction and the geometric errors of the turntable. The separation mathematical model of rotary axis's geometric error with this novel method is established, and the corresponding measurement algorithms containing base station calibration, measuring point determination based on the hybrid genetic algorithm, six geometric errors separation algorithm are deduced and then validated by numerical simulations. Meanwhile, the experiment concerning on detecting the rotary axis's geometric errors is implemented to further verify the feasibility and accuracy of the introduced approach.

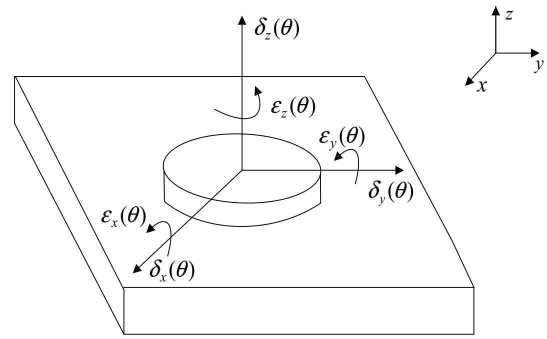

Fig. 1 Turntable's geometric errors rotating around z-axis

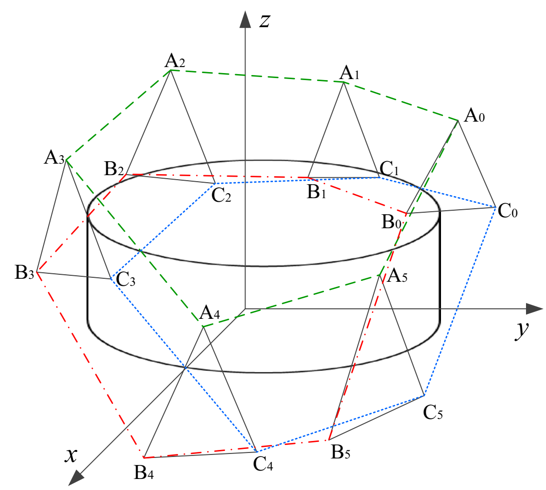

Fig. 2 The variation of vectors' direction during the motion of the turntable

2 The Relationship Between the Rotary Axis's Geometric and the Vector's Direction Variation

For a moving object, there exists 6 degrees of freedom. Figure 1 shows the turntable's geometric errors rotating around z-axis. Where,$\delta_x(\theta)$, $\delta_y(\theta)$, $\delta_z(\theta)$ refers to linear displacement errors, and $\varepsilon_x(\theta)$, $\varepsilon_y(\theta)$, $\varepsilon_z(\theta)$ refers to angular displacement errors around x-axis, y-axis, z-axis respectively [21].

There are three initial measuring points A_0, B_0 and C_0 mounted on the turntable as shown in Fig. 2. Because of the existing turntable's geometric errors, the direction of three vectors $\overrightarrow{A_0B_0}$, $\overrightarrow{B_0C_0}$, $\overrightarrow{C_0A_0}$ would be varied during the rotation.

As the turntable rotates θ angle around the z-axis, there exists a theoretical homogeneous transformation matrix shown in Eq. (1) [22]:

$$T_1 = \begin{bmatrix} \cos\theta & -\sin\theta & 0 & 0 \\ \sin\theta & \cos\theta & 0 & 0 \\ 0 & 0 & 1 & 0 \\ 0 & 0 & 0 & 1 \end{bmatrix} \tag{1}$$

The error transformation matrix during the rotation is defined as [23]:

$$T_2 = \begin{bmatrix} 1 & -\varepsilon_z(\theta) & \varepsilon_y(\theta) & \delta_x(\theta) \\ \varepsilon_z(\theta) & 1 & -\varepsilon_x(\theta) & \delta_y(\theta) \\ -\varepsilon_y(\theta) & \varepsilon_x(\theta) & 1 & \delta_z(\theta) \\ 0 & 0 & 0 & 1 \end{bmatrix} \tag{2}$$

For the initial measuring point $A_0(x_{a0}, y_{a0}, z_{a0})$, the actual coordinates of $A_i'(x_{ai}', y_{ai}', z_{ai}')$ with the turntable rotating different θ_i angle can be calculated as shown in Eq. (3).

$$\begin{bmatrix} x_{ai}' \\ y_{ai}' \\ z_{ai}' \end{bmatrix} = \begin{bmatrix} x_{a0}\cos\theta_i - x_{a0}\varepsilon_z(\theta_i)\sin\theta_i - y_{a0}\sin\theta_i - y_{a0}\varepsilon_z(\theta_i)\cos\theta_i + z_a\varepsilon_y(\theta_i) + \delta_x(\theta_i) \\ x_{a0}\varepsilon_z(\theta_i)\cos\theta_i + x_{a0}\sin\theta_i - y_{a0}\varepsilon_z(\theta_i)\sin\theta_i + y_{a0}\cos\theta - z_a\varepsilon_x(\theta_i) + \delta_y(\theta_i); \\ -x_{a0}\varepsilon_y(\theta_i)\cos\theta_i + x_{a0}\varepsilon_x(\theta_i)\sin\theta + y_{a0}\varepsilon_y(\theta_i)\sin\theta + y_{a0}\varepsilon_x(\theta_i)\sin\theta_i + z_a + \delta_z(\theta_i) \end{bmatrix} \tag{3}$$

Similarly, for the other initial measuring points B_0 and C_0, the actual coordinates of $B_i'(x_{bi}', y_{bi}', z_{bi}')$ and $C_i'(x_{ci}', y_{ci}', z_{ci}')$ with the turntable rotating θ_i angle can be also calculated. Then, the directions of the vectors $\overrightarrow{A_iB_i}$, $\overrightarrow{B_iC_i}$ and $\overrightarrow{C_iA_i}$ composed of the theoretical measuring points A_i, B_i and C_i can be expressed respectively as:

$$\overrightarrow{A_iB_i} = \begin{bmatrix} x_{b0}\cos\theta_i - y_{b0}\sin\theta_i - x_{a0}\cos\theta_i + y_a\sin\theta_i \\ x_{b0}\sin\theta + y_{b0}\cos\theta_i - x_{a0}\sin\theta - y_{a0}\cos\theta_i \\ z_{b0} - z_{a0} \end{bmatrix} \tag{4}$$

$$\overrightarrow{B_iC_i} = \begin{bmatrix} x_{c0}\cos\theta_i - y_{c0}\sin\theta_i - x_{b0}\cos\theta_i + y_{b0}\sin\theta_i \\ x_{c0}\sin\theta + y_{c0}\cos\theta_i - x_{b0}\sin\theta - y_{b0}\cos\theta_i \\ z_{c0} - z_{b0} \end{bmatrix} \tag{5}$$

$$\overrightarrow{C_iA_i} = \begin{bmatrix} x_{a0}\cos\theta_i - y_{a0}\sin\theta_i - x_{c0}\cos\theta_i + y_{c0}\sin\theta_i \\ x_{a0}\sin\theta + y_{a0}\cos\theta_i - x_{c0}\sin\theta - y_{c0}\cos\theta_i \\ z_{a0} - z_{c0} \end{bmatrix} \tag{6}$$

Accordingly, the directions of vectors $\overrightarrow{A_i'B_i'}$, $\overrightarrow{B_i'C_i'}$ and $\overrightarrow{C_i'A_i'}$ composed of the actual measuring points A_i', B_i', C_i' are determined. Then, the corresponding direction deviations of the vectors $\overrightarrow{A_iB_i}$, $\overrightarrow{B_iC_i}$, $\overrightarrow{C_iA_i}$ during the rotation can be obtained as follows:

$$\Delta\overrightarrow{A_iB_i} = \begin{bmatrix} \varepsilon_z(\theta_i)(-x_{b0}\sin\theta_i - y_{b0}\cos\theta_i + x_{a0}\sin\theta_i + y_{a0}\cos\theta_i) + \varepsilon_y(\theta_i)(z_{b0} - z_{a0}) \\ \varepsilon_z(\theta_i)(x_{b0}\cos\theta_i - y_{b0}\sin\theta_i - x_{a0}\cos\theta_i + y_{a0}\sin\theta_i) - \varepsilon_x(\theta_i)(z_{b0} - z_{a0}) \\ \varepsilon_x(\theta_i)(x_{b0}\sin\theta_i + y_{b0}\cos\theta_i - x_{a0}\sin\theta_i - y_{a0}\cos\theta_i) - \varepsilon_y(\theta_i)(x_{b0}\cos\theta_i - y_{b0}\sin\theta_i - x_{a0}\cos\theta_i + y_{a0}\sin\theta_i) \end{bmatrix} \tag{7}$$

$$\Delta\overrightarrow{B_iC_i} = \begin{bmatrix} \varepsilon_z(\theta_i)(-x_{c0}\sin\theta_i - y_{c0}\cos\theta_i + x_{b0}\sin\theta_i + y_{b0}\cos\theta_i) + \varepsilon_y(\theta_i)(z_{c0} - z_{b0}) \\ \varepsilon_z(\theta_i)(x_{c0}\cos\theta_i - y_{c0}\sin\theta_i - x_{b0}\cos\theta_i + y_{b0}\sin\theta_i) - \varepsilon_x(\theta_i)(z_{c0} - z_{b0}) \\ \varepsilon_x(\theta_i)(x_{c0}\sin\theta_i + y_{c0}\cos\theta_i - x_{b0}\sin\theta_i - y_{b0}\cos\theta_i) - \varepsilon_y(\theta_i)(x_{c0}\cos\theta_i - y_{c0}\sin\theta_i - x_{b0}\cos\theta_i + y_{b0}\sin\theta_i) \end{bmatrix} \tag{8}$$

$$\Delta\overrightarrow{C_iA_i} = \begin{bmatrix} \varepsilon_z(\theta_i)(-x_{a0}\sin\theta_i - y_{a0}\cos\theta_i + x_{c0}\sin\theta_i + y_{c0}\cos\theta_i) + \varepsilon_y(\theta_i)(z_{a0} - z_{c0}) \\ \varepsilon_z(\theta_i)(x_{a0}\cos\theta_i - y_{a0}\sin\theta_i - x_{c0}\cos\theta_i + y_{c0}\sin\theta_i) - \varepsilon_x(\theta_i)(z_{a0} - z_{c0}) \\ \varepsilon_x(\theta_i)(x_{a0}\sin\theta_i + y_{a0}\cos\theta_i - x_{c0}\sin\theta_i - y_{c0}\cos\theta_i) - \varepsilon_y(\theta_i)(x_{a0}\cos\theta_i - y_{a0}\sin\theta_i - x_{c0}\cos\theta_i + y_{c0}\sin\theta_i) \end{bmatrix} \tag{9}$$

From Eq. (7) to (9), it can be obviously seen that the direction variations of $\overrightarrow{A_iB_i}$, $\overrightarrow{B_iC_i}$, $\overrightarrow{C_iA_i}$ during the rotation are merely related to angular displacement errors rather than linear displacement errors. According to this characteristic, three angular displacement errors $\varepsilon_x(\theta)$, $\varepsilon_y(\theta)$ and $\varepsilon_z(\theta)$ can be firstly identified on the basis of the direction variation of a series of vectors, and three line displacement errors $\delta_x(\theta)$, $\delta_y(\theta)$ and $\delta_z(\theta)$ would be separated at last.

3 Measurement Principle and Algorithm

3.1 Measurement Principle

The coordinates of target point can be measured with the laser tracking system based on spherical coordinate, and the measuring accuracy is mostly affected by the angle measurement error [24, 25]. In order to overcome the effect of introduced angle measurement error, the multi-station and time-sharing method is applied. The target point can therefore be determined successively by collecting corresponding ranging data of laser tracker at different base stations based on the GPS principle. The direction of a series of vectors composed of adjacent measuring points during the rotation of turntable will be measured, then the turntable's geometric errors can be separated respectively. In the measurement, quick and accurate calibration of each base station is critical, and then a precision NC turntable is designed to ensure it. Its axial and radial runout are less than 0.3 μm, meanwhile its position accuracy is $\pm 2''$ with repeatability of $\pm 1''$. The cat eye is set on the designed turntable and rotates accurately with different angles driven by the turntable. By using laser tracker to detect the rotary motion of the precision NC turntable, the accurate position of each base station will be calibrated and obtained. The geometric error measurement principle of the turntable by combining laser tracker with the designed precision turntable is shown in Figs. 3, and 4 gives the corresponding flowchart with this proposed method.

3.2 Measurement Algorithm

With this approach, the base station calibration and measurement point determination algorithms are mainly involved and studied [26, 27].

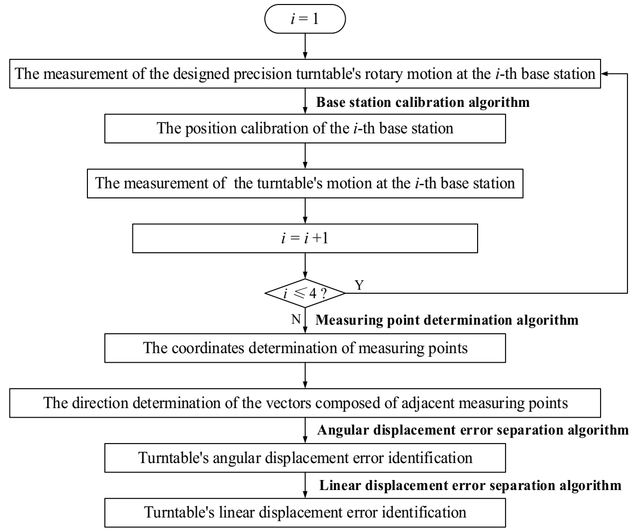

Fig. 4 Measurement and identification process of turntable's geometric error

3.2.1 Base Station Calibration

According to the introduced measurement principle in Sect. 3.1, the corresponding calibration model of base station can be constructed as shown in Fig. 5. Where, Q_1, $Q_2 \ldots Q_n$ are defined as the measuring points on the turntable, and P represents the position of base station.

Currently, the measurement principles of common laser trackers can be divided into two categories. For the laser trackers such as Leica, Faro and API, these instruments usually have the coordinate measurement function, and the absolute distance between the target point and the center of tracking mirror can be measured. For these laser trackers,

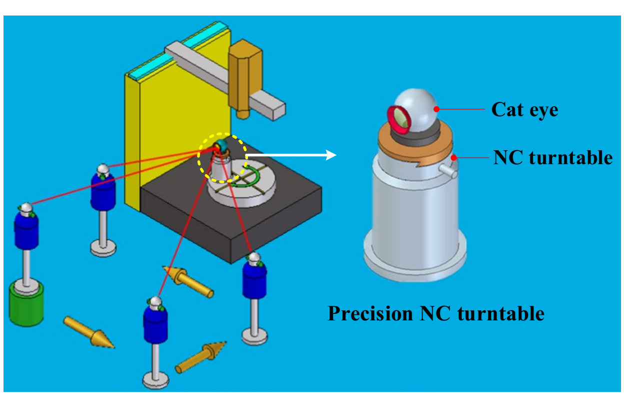

Fig. 3 Geometric error measurement principle of the turntable by combining laser tracker with the designed turntable

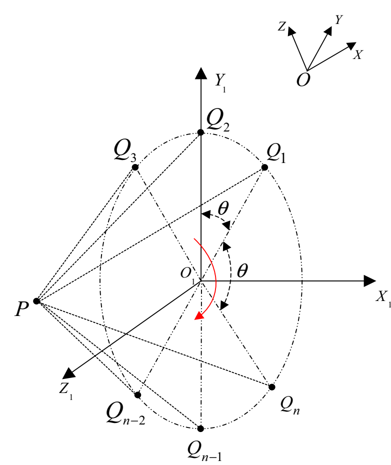

Fig. 5 Calibration mode of the base station

the calibration equation of base station $P_1(x_{p1}, y_{p1}, z_{p1})$ can be established as follows:

$$\begin{cases} \sqrt{(x_{p1} - R\cos\theta_1)^2 + (y_{p1} - R\sin\theta_1)^2 + z_{p1}^2} = l_{11} \\ \sqrt{(x_{p1} - R\cos\theta_2)^2 + (y_{p1} - R\sin\theta_2)^2 + z_{p1}^2} = l_{12} \\ \vdots \\ \sqrt{(x_{p1} - R\cos\theta_i)^2 + (y_{p1} - R\sin\theta_i)^2 + z_{p1}^2} = l_{1i} \end{cases} \tag{10}$$

where R is defined as the distance between the center of designed turntable and cat eye, and θ_i represents different rotating angles. l_{1i} represents the corresponding ranging data at each measuring point.

For the Etalon laser tracker, it is not available for angle measurement as well as the initial distance measurement between the target point and the center of tracking mirror. Thus, this distance value needs to be calibrated in the measurement. The corresponding calibration equation of base station $P_1(x_{p1}, y_{p1}, z_{p1})$ by Etalon laser tracker can also be attained:

$$\begin{cases} \sqrt{(x_{p1} - R\cos\theta_1)^2 + (y_{p1} - R\sin\theta_1)^2 + z_{p1}^2} = L_1 + \Delta l_{11} \\ \sqrt{(x_{p1} - R\cos\theta_2)^2 + (y_{p1} - R\sin\theta_2)^2 + z_{p1}^2} = L_1 + \Delta l_{12} \\ \vdots \\ \sqrt{(x_{p1} - R\cos\theta_i)^2 + (y_{p1} - R\sin\theta_i)^2 + z_{p1}^2} = L_1 + \Delta l_{1i} \end{cases} \tag{11}$$

where L_1 is the distance between the center of tracking mirror and initial measuring point, and Δl_{1i} is defined as the variation of the relative distance at different measuring points.

Equations (10) and (11) are nonlinear redundant equations, and how to solve these equations is a critical issue [28].

Genetic algorithm is a smart optimization algorithm to simulate the biological evolution [29, 30]. It is an iterative and adaptive probabilistic search method based on the principle of natural selection and genetic mechanism, which has been widely adopted in the optimization field [31]. However, premature convergence is prone to occur in the process of genetic manipulation, resulting in poor local search ability for genetic algorithm. When solving a large and complex problem, only local optimal solution could be often obtained [32].

In view of good local searching ability for the simplex method, the hybrid genetic algorithm combining simplex method with traditional genetic algorithm is adopted to calibrate the positions of base stations and determine the coordinates of each measuring point [33]. Then the good local and global searching ability can both be preserved for the new hybrid genetic algorithm, which can effectively overcome the deficiency of traditional genetic algorithm and further improve the calculation accuracy.

3.2.2 Measuring Point Determination

The rotation of the turntable can be measured after the base station calibration. In the same way as base station calibration, the equations for measuring point determination can also be established, and the coordinate of each measuring point can be obtained with the hybrid genetic algorithm mentioned above. Finally, the directions of a series of vectors composed of the adjacent measuring points can be easily determined.

4 Geometric Error Identification of the Turntable

The geometric error identification of the turntable consists of two parts: (1) angular displacement error identification; (2) linear displacement error identification.

4.1 Angular Displacement Error Identification

It is assumed that there exist three initial measuring points $A_0(x_{a0}, y_{a0}, z_{a0})$, $B_0(x_{b0}, y_{b0}, z_{b0})$ and $C_0(x_{c0}, y_{c0}, z_{c0})$ at the initial position of the turntable as shown in Fig. 2. With different rotating angles of the turntable, the theoretical and actual coordinates of a series of measuring points are assumed as: $A_i(x_{ai}, y_{ai}, z_{ai})$, $B_i(x_{bi}, y_{bi}, z_{bi})$, $C_i(x_{ci}, y_{ci}, z_{ci})$, $A_i'(x_{ai}', y_{ai}', z_{ai}')$, $B_i'(x_{bi}', y_{bi}', z_{bi}')$ and $C_i'(x_{ci}', y_{ci}', z_{ci}')$ respectively.

At the initial position, the direction of vectors $\overrightarrow{AB}$, $\overrightarrow{BC}$ and $\overrightarrow{CA}$ are:

$$\begin{aligned} \overrightarrow{AB} &= (x_{b0} - x_{a0}, y_{b0} - y_{a0}, z_{b0} - z_{a0}), \\ \overrightarrow{BC} &= (x_{c0} - x_{b0}, y_{c0} - y_{b0}, z_{c0} - z_{b0}), \\ \overrightarrow{CA} &= (x_{a0} - x_{c0}, y_{a0} - y_{c0}, z_{a0} - z_{c0}). \end{aligned}$$

During the rotation of turntable, the direction of actual vectors $\overrightarrow{A_i'B_i'}$, $\overrightarrow{B_i'C_i'}$, and $\overrightarrow{C_i'A_i'}$ are:

$$\begin{aligned} \overrightarrow{A_i'B_i'} &= (x_{bi}' - x_{ai}', y_{bi}' - y_{ai}', z_{bi}' - z_{ai}'), \\ \overrightarrow{B_i'C_i'} &= (x_{ci}' - x_{bi}', y_{ci}' - y_{bi}', z_{ci}' - z_{bi}'), \\ \overrightarrow{C_i'A_i'} &= (x_{ai}' - x_{ci}', y_{ai}' - y_{ci}', z_{ai}' - z_{ci}'). \end{aligned}$$

According to the motion transformation matrix of turntable, the following relationship between $\overrightarrow{AB}$ and $\overrightarrow{A_i'B_i'}$ should exist.

$$\begin{bmatrix} x'_{bi} - x'_{ai} \\ y'_{bi} - y'_{ai} \\ z'_{bi} - z'_{ai} \\ 1 \end{bmatrix} = \begin{bmatrix} 1 & -\varepsilon_z(\theta_i) & \varepsilon_y(\theta_i) & 0 \\ \varepsilon_z(\theta_i) & 1 & -\varepsilon_x(\theta_i) & 0 \\ -\varepsilon_y(\theta_i) & \varepsilon_x(\theta_i) & 1 & 0 \\ 0 & 0 & 0 & 1 \end{bmatrix} \begin{bmatrix} \cos\theta_i & -\sin\theta_i & 0 & 0 \\ \sin\theta_i & \cos\theta_i & 0 & 0 \\ 0 & 0 & 1 & 0 \\ 0 & 0 & 0 & 1 \end{bmatrix} \begin{bmatrix} x_{b0} - x_{a0} \\ y_{b0} - y_{a0} \\ z_{b0} - z_{a0} \\ 1 \end{bmatrix} \tag{12}$$

Then, it can be deduced that:

$$\begin{cases} x'_{bi} - x'_{ai} = \varepsilon_y(\theta_i)(z_{b0} - z_{a0}) + \varepsilon_z(\theta_i)(x_{a0}\sin\theta_i - x_{b0}\sin\theta_i + y_{a0}\cos\theta_i - y_{b0}\cos\theta_i) + x_{b0}\cos\theta_i - x_{a0}\cos\theta_i - y_{b0}\sin\theta_i + y_{a0}\sin\theta \\ y'_{bi} - y'_{ai} = \varepsilon_x(\theta_i)(z_{a0} - z_{b0}) + \varepsilon_z(\theta_i)(x_{b0}\cos\theta_i - x_{a0}\cos\theta_i - y_{b0}\sin\theta_i + y_{a0}\sin\theta_i) + x_{b0}\sin\theta_i + y_{b0}\cos\theta_i - x_{a0}\sin\theta_i - y_{a0}\cos\theta \\ z'_{bi} - z'_{ai} = \varepsilon_x(\theta_i)(x_{b0}\sin\theta_i - x_{ao}\sin\theta_i + y_{b0}\cos\theta_i - y_{a0}\cos\theta_i) - \varepsilon_y(\theta_i)(x_{b0}\cos\theta_i - x_{a0}\cos\theta_i - y_{b0}\sin\theta_i + y_{a0}\sin\theta_i) + z_{b0} - z_{a0} \end{cases} \tag{13}$$

In the same way, the relationship between the vectors $\overrightarrow{BC}$ and $\overrightarrow{B'_iC'_i}$, as well as $\overrightarrow{CA}$ and $\overrightarrow{C'_iA'_i}$ can also be established, then the equation concerning angular displacement errors $\varepsilon_x(\theta)$, $\varepsilon_y(\theta)$ and $\varepsilon_z(\theta)$ will be obtained. By solving this equation, three angular displacement errors during the rotation of turntable can be separated.

4.2 Linear Displacement Error Identification

During the rotation of turntable, the volumetric position error of each measuring point consists of two parts: one part is caused by the line displacement error, and the other part is caused by the angular displacement error. The corresponding position deviation induced by the identified angular displacement errors can be calculated at each measuring point. For the measuring point A_i, it is assumed that the position deviations in the three directions caused by the angular displacement errors are t_{axi}, t_{ayi} and t_{azi} respectively. Then the equality relationship on linear displacements errors exists:

$$\begin{cases} x'_{ai} - x_{ai} = \delta_x(\theta_i) + t_{axi} \\ y'_{ai} - y_{ai} = \delta_y(\theta_i) + t_{ayi} \\ z'_{ai} - z_{ai} = \delta_z(\theta_i) + t_{azi} \end{cases} \tag{14}$$

Similarly, the equations concerning the point B_i and C_i can be also established, then we can obtain the following equations:

$$\begin{cases} x'_{ai} - x_{ai} = \delta_x(\theta_i) + t_{axi} \\ y'_{ai} - y_{ai} = \delta_y(\theta_i) + t_{ayi} \\ z'_{ai} - z_{ai} = \delta_z(\theta_i) + t_{azi} \\ x'_{bi} - x_{bi} = \delta_x(\theta_i) + t_{bxi} \\ y'_{bi} - y_{bi} = \delta_y(\theta_i) + t_{byi} \\ z'_{bi} - z_{bi} = \delta_z(\theta_i) + t_{bzi} \\ x'_{ci} - x_{ci} = \delta_x(\theta_i) + t_{cxi} \\ y'_{ci} - y_{ci} = \delta_y(\theta_i) + t_{cyi} \\ z'_{ci} - z_{ci} = \delta_z(\theta_i) + t_{czi} \end{cases} \tag{15}$$

Three linear displacement errors $\delta_x(\theta)$, $\delta_y(\theta)$ and $\delta_z(\theta)$ can be separated by solving Eq. (15). In the above process, the identifications of angular and linear displacement errors of the rotary axis are decoupled, which is conducive to reduce the complexity of identification model and facilitate the accurate separation for each error.

5 Simulation for Measurement and Geometric Error Identification Algorithms of Rotary Axis

In order to validate the derived algorithms, the simulations regarding the measurement and geometric error identification algorithms are performed as follows.

5.1 Simulation for Measurement Algorithm of Rotary Axis

There exists certain similarity between the involved base station calibration and measuring point determination algorithms. Meanwhile, the measurement precision of this method largely depends on the calibration accuracy of base station. Therefore, the simulations and analysis on the base station calibration are typically given. Firstly, the positions of each base station are assumed as: $P_1(800, 600, 1200)$, $P_2(800, 1800, 1200)$, $P_3(-1200, 600, 2200)$, $P_4(-1200, 1800, 2200)$. The distance between the center of turntable and cat eye is 200 mm, and a measuring point is set for rotating each θ=20° of the turntable. The following simulations are conducted under two conditions:

Table 1 Calibration deviations of P_1 with the genetic algorithm mm

Calibration deviations	Δx	Δy	Δz
First time	−0.0085	−0.0053	−0.0082
Second time	−0.0045	−0.0039	−0.0069
Third time	0.0028	0.0020	0.0033

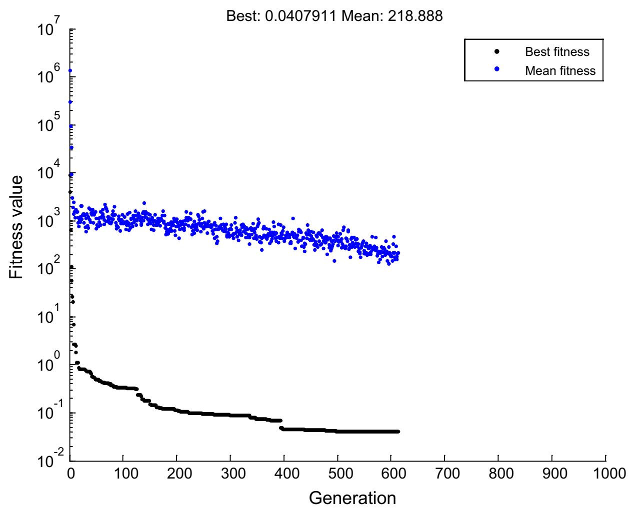

Fig. 6 Distribution of best fitness and mean fitness in the evolution

Table 2 Calibration deviations of P_1 with the hybrid genetic algorithm mm

Calibration deviations	Δx	Δy	Δz
First time	4.4×10^{-6}	7.1×10^{-6}	1.8×10^{-5}
Second time	-1.3×10^{-5}	-5.1×10^{-6}	-6.8×10^{-6}
Third time	1.5×10^{-5}	1.1×10^{-5}	2.3×10^{-6}

Table 3 Calibration uncertainty of P_1 with genetic algorithm and hybrid genetic algorithm mm

Algorithm	Calibration uncertainty		
	x	y	z
Genetic algorithm	0.0047	0.0032	0.0051
Hybrid genetic algorithm	1.2×10^{-5}	6.9×10^{-6}	1.0×10^{-5}

considering the rotation error of the designed turntable or not.

(1) Regardless of the turntable rotation error

The turntable can accurately rotate different angles according to the command without considering its motion error. The genetic algorithm is adopted to calibrate the base station. The main parameters involved in the calculation are: population size 150, deviations between initial parameters range and their true values ± 0.1 mm, crossover rate 0.6 and mutation rate 0.02 etc. Table 1 shows the calibration deviations of base station P_1 with the genetic algorithm for three calculations.

As shown in Table 1, large calibration deviations of base stations and the poor repeatability of calibration results for different times are presented. This can be attribute to random procedure used in the traditional genetic algorithm for searching the optimal solution. Meanwhile, prematurity phenomenon and poor local searching ability are both inevitable deficiencies for this algorithm.

To overcome the deficiencies, the constituted hybrid genetic algorithm mentioned above is adopted. Figure 6 illustrates the distribution of best fitness and mean fitness in the evolution, and the corresponding calibration deviations with this algorithm for three calculations are given in Table 2.

It can be seen from Table 2 that, the calibration accuracy and repeatability are greatly enhanced compared with the traditional genetic algorithm, which is effective for multiple calculations. Taking base station P_1 as an example, Table 3 shows the calibration uncertainty of P_1 with genetic algorithm and hybrid genetic algorithm on the basis of Monte Carlo method respectively.

From Table 3, the calibration uncertainty of base station is smaller with the hybrid genetic algorithm, and the stability of the solution is good. Similar conclusions can be also obtained at other base stations. Accordingly, the calibration

Table 4 Calibration deviations of four base stations by the hybrid genetic algorithm mm

Base station	Calibration deviations		
	Δx	Δy	Δz
P_1	1.8×10^{-6}	4.5×10^{-6}	1.2×10^{-5}
P_2	1.8×10^{-5}	4.0×10^{-5}	2.3×10^{-5}
P_3	-2.1×10^{-5}	8.9×10^{-6}	3.1×10^{-5}
P_4	2.8×10^{-5}	-4.1×10^{-5}	-4.7×10^{-5}

Table 5 Calibration deviations of P_1 by the hybrid genetic algorithm with different initial ranges mm

Initial range	Calibration deviations		
	Δx	Δy	Δz
1	1.8×10^{-6}	4.5×10^{-6}	1.2×10^{-5}
2	4.5×10^{-5}	4.8×10^{-5}	8.7×10^{-5}
3	2.0×10^{-6}	-6.2×10^{-7}	2.6×10^{-6}
4	-1.5×10^{-5}	-1.1×10^{-5}	-2.7×10^{-5}

Table 6 Calibration deviations of four base stations under the first condition mm

Base station	Calibration deviations		
	Δx	Δy	Δz
P_1	-4.6×10^{-4}	-2.2×10^{-4}	-5.0×10^{-4}
P_2	-2.5×10^{-4}	-8.9×10^{-4}	0.0012
P_3	-3.2×10^{-4}	-6.3×10^{-4}	0.0011
P_4	0.0014	-0.0016	-9.3×10^{-4}

deviations of four base stations with this algorithm can be seen in Table 4.

Regardless of the rotation error of the designed turntable, accurate position calibration for each base station can be realized with small deviations by this hybrid algorithm.

In the base station calibration, the selected initial ranges of calibration parameters have certain effect on the calculation results. Here, the deviations between initial ranges of parameters and their true values are assumed as ± 0.1 mm, ± 10 mm, ± 100 mm and ± 1000 mm. Here, ± 0.1 mm, ± 10 mm, ± 100 mm and ± 1000 mm are defined as initial range 1, 2, 3, 4 respectively. In view of these different initial ranges, the corresponding simulations are conduced. Taking the calibration of base station P_1 as an instance,the calibration deviations by the hybrid genetic algorithm with different initial ranges for the calibration parameters are shown in Table 5.

Less fluctuation in calibration results for different initial values of calibration parameter indicates the hybrid genetic algorithm is insensitive to the selected initial ranges of calibration parameters and has a certain robustness.

(2) Considering the turntable rotation error

There exist certain deviations between the theoretical and actual rotation angles of the designed turntable. For ease of analysis, the position error of the designed turntable is supposed to obey random normal distribution within [0, 3″] and [0, 5″] respectively. In addition, the ranging error of laser tracker is also considered to obey random normal distribution within [0, 1 μm]. Table 6 gives the calibration deviations of four base stations under the first condition.

In Table 6, the calibration deviations are small under the condition, suggesting the base station calibration using the hybrid genetic algorithm is feasible and effective. Further simulations and analysis show the calibration accuracy gradually increases with increased position error of the turntable.

Table 7 Identification deviations of six geometric errors under different random error distributions

Identification deviation	Random error distribution	
	1	2
$\Delta\delta_x(\theta)$/mm	0.00025	0.00040
$\Delta\delta_y(\theta)$/mm	−0.00042	−0.00067
$\Delta\delta_z(\theta)$/mm	−0.00053	−0.00085
$\Delta\varepsilon_x(\theta)$/rad	2.2×10^{-6}	3.2×10^{-6}
$\Delta\varepsilon_y(\theta)$/rad	3.8×10^{-6}	6.5×10^{-6}
$\Delta\varepsilon_z(\theta)$/rad	3.4×10^{-6}	5.2×10^{-6}

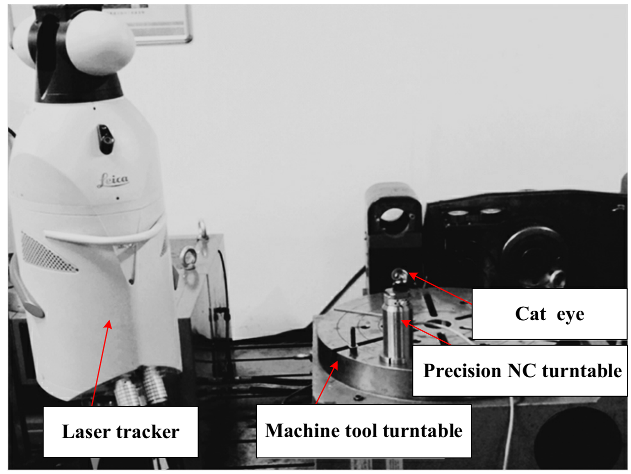

Fig. 7 Geometric error identification of the turntable

5.2 Simulation for Geometric Error Identification Algorithm of Rotary Axis

Taking the geometric error identification of rotary axis with rotating 30° as an example, the validation of the derived error identification algorithm is carried out. Firstly, each geometric error of the turntable with rotating 30° is assumed as: $\delta_x(\theta) = 0.030$ mm, $\delta_y(\theta) = 0.020$ mm, $\delta_z(\theta) = 0.010$ mm, $\varepsilon_x(\theta) = 2.0 \times 10^{-5}$ rad, $\varepsilon_y(\theta) = 3.5 \times 10^{-5}$ rad and $\varepsilon_z(\theta) = 4.5 \times 10^{-5}$ rad respectively. The simulations are then conducted under two cases: without or with considering the impact of random error during the rotation of turntable.

Under the first case, six geometric errors of turntable can be exactly separated. The maximum identification deviation is 1.0×10^{-14} mm for $\delta_y(\theta)$.

Under the second case, a random error is introduced to each measuring point's theoretical motion error. To simplify calculations, the random error is supposed to obey random normal distribution within [0, 3 μm] and [0, 5 μm]. Here, [0,

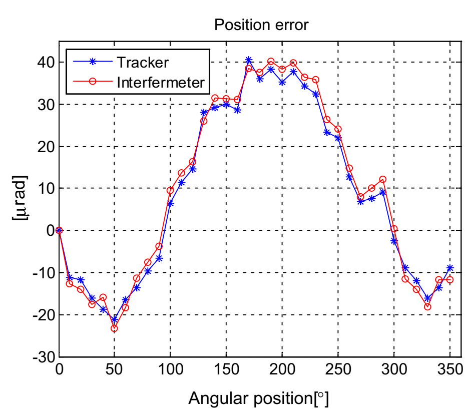

Fig. 8 Comparision of two mesurment methods

3 μm], [0, 5 μm] represents case 1 and 2 respectively. The identification deviations of six geometric errors under the two cases are listed in Table 7.

From Table 7, the corresponding identification deviations of six geometric errors are relatively small for different random error distributions, revealing the feasibility of the derived identification algorithm.

6 Experimental Verification

The identification of geometric errors of the turntable with laser tracker is implemented by measuring vectors' direction variations during the rotation as seen in Fig. 7.

The rotation of the turntable is successively measured by tracking at four different base stations. At each base station, the turntable rotates and stops at each interval of 10°, and the corresponding distance data of laser tracker is recorded every 120° of the turntable rotation. Entire measurement takes about 3 h with high efficiency. Each geometric error of rotary axis can therefore be separated through the proposed measurement algorithm and error identification algorithm.

To further validate the feasibility of the new approach, taking the identification of the position error as a case, the identification results by the proposed approach are compared to that by laser interferometer cooperating with Renishaw rotary measuring system RX10 as shown in Fig. 8.

From Fig. 8, it can be seen that the variation trend of the turntable's position error curves measured by two methods are basically consistent, and the corresponding deviations at different measuring points are small. So the proposed method is feasible and effective.

Adopting the proposed method, the measurement uncertainty will be affected by time-sharing measurement, ranging error of laser tracker, designed turntable's precision and repeatability, surrounding environment etc. In the measurement, the motion trajectory of turntable is measured by laser tracker at different base stations. Due to adopting the time-sharing measurement principle, the motion trajectories of the turntable measured at different base stations are different. In order to reduce the impact of time-sharing measurement, the motion of turntable will be measured for multiple times at each base station, then this error can be significantly reduced. To reduce the influence of the ranging error of laser tracker, the laser tracker can be set as close as possible to the tested turntable on the premise of keeping the measuring optical path uninterrupted. Meanwhile, the environmental compensation for temperature, pressure and humidity will ensure the ranging accuracy of laser tracker. In addition, the position precision and repeatability of the designed turntable have certain influence on the base station calibration. The designed turntable should have a certain precision requirement to ensure the measurement precision and repeatability. This proposed method can achieve the rapid measurement of the turntable's error. Owing to the short measuring time, the measurement environment changes little, which has smaller effect on the measurement results.

7 Conclusions

(1) A novel identification method with laser tracker is proposed to realize rapid and accurate separation of geometric errors of the rotary axis of multi-axis machine tool.
(2) The identification mathematical model of rotary axis's geometric error is established on the basis of measuring the direction variations of vectors. The measurement algorithms containing the base station calibration, the measuring point determination based on the hybrid genetic algorithm, as well as six geometric errors separation algorithm involving angular errors and displacement errors are deduced respectively and validated by simulations.
(3) The geometric error measurement of the turntable by this method is completed in about 3 h, and then six geometric errors can be identified efficiently. Meanwhile, identifying the turntable's position error as a case, the identification results by the proposed method are compared to that by laser interferometer cooperating with Renishaw rotary measuring system, which further confirms the feasibility of the introduced new approach.

Acknowledgements This research was supported by State Key Laboratory of Precision Measuring Technology and Instruments (Tianjin University) (Grant No. pilab1904), Fundamental Research Funds for the Central Universities (Grant No. 2682017CX025).

References

1. Jian, G., Yueping, C., Haixiang, D., et al. (2013). In-situ inspection error compensation for machining accuracy improvement of complex components. *Journal of Mechanical Engineering, 49*(19), 133–143.
2. Qin, J. Y., Jia, Z. Y., Ma, J. W., et al. (2018). Kinematical performance prediction method for rotary axes of 5-axis machine tool in processing of complex curved surface. *International Journal of Industrial and Systems Engineering, 28*(2), 178–192.
3. Flemmer, J., Ross, I., Willenborg, E., et al. (2015). Machine tool and CAM-NC data chain for laser polishing complex shaped parts. *Advanced Engineering Materials, 17*(3), 260–267.
4. Schwenke, H., Schmitt, R., Jatzkowski, P., et al. (2009). On-the-fly calibration of linear and rotary axes of machine tools and CMMs using a tracking interferometer. *CIRP Annals—Manufacturing Technology, 58*(1), 477–480.
5. Wang, Y., Peng, X., Hu, H., et al. (2015). Identification and compensation for offset errors on the rotary axes of a multi-axis

Magnetorheological Finishing machine tool. *The International Journal of Advanced Manufacturing Technology, 78*(9–12), 1743–1749.
6. Jiang, X., & Cripps, R. J. (2015). A method of testing position independent geometric errors in rotary axes of a five-axis machine tool using a double ball bar. *International Journal of Machine Tools and Manufacture, 89,* 151–158.
7. Wang, J., Guo, J., Zhou, B., et al. (2012). The detection of rotary axis of NC machine tool based on multi-station and time-sharing measurement. *Measurement, 45*(7), 1713–1722.
8. Acosta, D., Albajez, J. A., & Velázquez, J. (2015). The use of a laser tracker and a self-centring probe for rotary axis verification. *Procedia engineering, 132,* 748–755.
9. Lee, J.-C., Lee, H.-H., & Yang, S.-H. (2016). Total measurement of geometric errors of a three-axis machine tool by developing a hybrid technique. *Ininternational Journal of Precision Engineering and Manufacturing, 17,* 427–432.
10. Lee, K.-I., & Yang, S.-H. (2013). Robust measurement method and uncertainty analysis for position-independent geometric errors of a rotary axis using a double ball-bar. *International Journal of Precision Engineering and Manufacturing, 14,* 231–239.
11. Zargarbashi, S. H. H., & Rene, M. (2007). A predictive maintenance method for rotary axes of five-axis machine tools. In *Canadian Congress of Applied Mechanics* (Vol. 21).
12. Ibaraki, S., Oyama, C., & Otsubo, H. (2011). Construction of an error map of rotary axes on a five-axis machining center by static R-test. *International Journal of Machine Tools and Manufacture, 51*(3), 190–200.
13. Aguado, S., Samper, D., Santolaria, J., et al. (2012). Identification strategy of error parameter in volumetric error compensation of machine tool based on laser tracker measurements. *International Journal of Machine Tools and Manufacture, 53*(1), 160–169.
14. Pan, B. Z., Song, Y. M., Wang, P., et al. (2014). Laser tracker based rapid home position calibration of a hybrid robot. *Journal of Mechanical Engineering, 50*(1), 31–37.
15. Zhang, Z., Hu, H., & Liu, X. (2011). Measurement of geometric error of machine tool guideway system based on laser tracker. *Chinese Journal of lasers, 38*(9), 1–6.
16. Lin, J. R., Zhu, J. G., Zhang, H. L., et al. (2012). Field evaluation of laser tracker angle measurement error. *Chinese Journal of Scientific Instrument, 33*(2), 463–468.
17. Bai, P. J., Xue, N., Liu, S., et al. (2016). Angular calibration method of precision rotating platform based on laser tracker. *Journal of South China University of Technology (Natural Science Edition), 44*(1), 100–107.
18. Kenta, U., Ryosyu, F., Sonko, O., et al. (2005). Geometric calibration of a coordinate measuring machine using a laser tracking system. *Measurement Science and Technology, 16*(12), 2466–2472.
19. Aguado, S., Santolaria, J., & Samper, D. (2014). Study of self-calibration and multilateration in machine tool volumetric verification for laser tracker error reductions. *Proceedings of the Institution of Mechanical Engineers Part B Journal of Engineering Manufacture, 228*(7), 659–672.
20. Schwenke, H., Franke, M., Hannaford, J., et al. (2005). Error mapping of CMMs and machine tools by a single tracking interferometer. *CIRP Annals-Manufacturing Technology, 54*(1), 475–478.
21. Cheng, Q., Zhao, H. W., Cai, L., et al. (2014). Influence analysis of machine tool's turntable angle errors to the roundness of machined hole. *Applied Mechanics and Materials, Frontiers of Manufacturing and Design Science IV, 496–500,* 816–822.
22. Yongdong, L., Jia, W. A. N. G., & Jinwen, L. (1999). Self-calibration of multi-station laser tracking system for dynamic geometric measurement. *Optical Technique, 3,* 25–27.
23. Kiridena, V., & Ferreira, P. M. (1993). Mapping the effects of positioning errors on the volumetric accuracy of five-axis CNC machine tools. *International Journal of Machine Tools and Manufacture, 33*(3), 417–437.
24. Predmore, C. R. (2010). Bundle adjustment of multi-position measurements using the Mahalanobis distance. *Precision Engineering, 34*(1), 113–123.
25. Zhang, D., Rolt, S., & Maropoulos, P. G. (2005). Modelling and optimization of novel laser multilateration schemes for high-precision applications. *Measurement Science and Technology, 16*(12), 2541–2547.
26. Lin, G., & Li, X. (2009). Site measuring accuracy testing of laser tracker. *Journal of Beijing University of Aeronautics and Astronautics, 35*(5), 612–614.
27. Guoxiong, Z., Yongbing, L., Xinghua, L., et al. (2003). Four-Bearn Laser Tracking Interferometer System for Three-Dimensional Coordinate Measurement. *Acta Optica Sinica, 23*(9), 1030–1036.
28. Kudryashov, N. A. (2012). One method for finding exact solutions of nonlinear differential equations. *Communications in Nonlinear Science and Numerical Simulation, 17*(6), 2248–2253.
29. Israeli, E., & Gilad, E. (2018). Novel genetic algorithm for loading pattern optimization based on core physics heuristics. *Annals of Nuclear Energy, 118,* 35–48.
30. Jiadong, Z., Shaohui, S., Chen, C., et al. (2018). Improved interactive genetic algorithm for product configurationdesign. *China Mechanical Engineering, 29*(2), 2474–2478.
31. Jerald, J., Asokan, P., Saravanan, R., et al. (2006). Simultaneous scheduling of parts and automated guided vehicles in an FMS environment using adaptive genetic algorithm. *International Journal of Advanced Manufacturing Technology, 29*(5), 584–589.
32. Pizzuti, C. (2011). A multiobjective genetic algorithm to find communities in complex networks. *IEEE Transactions on Evolutionary Computation, 16*(3), 418–430.
33. He, Y., Wu, Y. G., Tian, J. L., et al. (2014). Image restoration of depth of field extension imaging system based on genetic algorithm. *Applied Mechanics and Materials, Advanced Engineering Solutions, 539,* 131–135.

Publisher's Note Springer Nature remains neutral with regard to jurisdictional claims in published maps and institutional affiliations.

Jindong Wang Associate professor at the School of Mechanical Engineering, Southwest Jiaotong University, Chengdu, China. His research interests include digital measurement technology and data processing.

Cong Cheng M.Sc. candidate at the School of Mechanical Engineering, Southwest Jiaotong University, Chengdu, China. His research interests concentrate on date processing and bionic design.

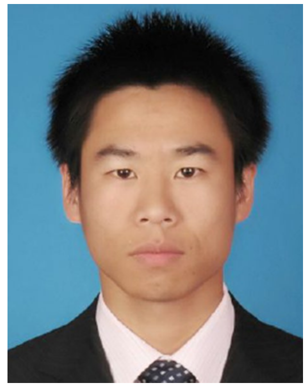

Haitao Li Ph.D. in the Department of Mechanical Engineering, Shaanxi University of Science & Technology, Xi'an, China. His research interest is precision measurement.